Catalysis Today 445 (2025) 115090

Contents lists available at ScienceDirect

Catalysis Today

journal homepage: www.elsevier.com/locate/cattod

Metal-free carbon nitride polymeric films for the synthesis of valuable organics using a novel mesostructured photoreactor

Dânia S.M. Constantino [a,b,1,2], Joana C. Lopes [a,b,1], Rafael C. Carneiro [a,b], José C.B. Lopes, [a,b], Madalena M. Dias [a,b], Joaquim L. Faria [a,b], Cláudia G. Silva [a,b,*]

[a] Laboratory of Separation and Reaction Engineering – Laboratory of Catalysis and Materials (LSRE-LCM), Faculty of Engineering, University of Porto, Rua Dr. Roberto Frias, Porto 4200-465, Portugal

[b] ALiCE - Associate Laboratory in Chemical Engineering, Faculty of Engineering, University of Porto, Rua Dr. Roberto Frias, Porto 4200-465, Portugal

ARTICLE INFO

Keywords:
Immobilised photocatalytic system
Biodegradable polymers
Graphitic carbon nitride
Micro-meso photoreactors
Light-emitting diodes
Aldehyde synthesis

ABSTRACT

Immobilised photocatalytic systems can strongly contribute to attaining more sustainable chemical processes, reducing downstream units for photocatalyst recovery and purification of the target molecules. On the other hand, it is known that this kind of photocatalytic system usually presents higher mass transfer resistance when compared with slurries and, consequently, slower kinetics. Besides, this can be even more limited for chemical synthesis using eco-friendly conditions, where combining the photocatalytic material with the best reactor design plays a fundamental role in the process efficiency. In this work, a micro-meso structured photoreactor was used to overcome these limitations, providing a large surface area per reaction volume and a higher illumination homogeneity through the entire reactor using a compact LED system. Several photocatalytic films were developed, combining different amounts of a metal-free photocatalyst (graphitic carbon nitride) with a biodegradable polymer matrix (sodium alginate). The catalytic performance was evaluated in the synthesis of aromatic aldehydes (anisaldehyde, tolualdehyde, benzaldehyde, vanillin, and piperonal from the photocatalytic oxidation of the corresponding, anisyl-, toluyl-, benzyl-, vanillyl- and piperonyl alcohols. All experimental runs were carried out under mild operation conditions, using water as solvent, room temperature and atmospheric pressure, and natural pH. The maximum performance in terms of yield was attained in the following order: anisaldehyde > tolualdehyde > piperonal > benzaldehyde > vanillin. A novel approach for photocatalytic organic synthesis with a low carbon footprint and reduced energy requirements is proposed. Moreover, the results provided in this work open a new window for the development of sustainable photocatalytic organic processes in continuous mode operation.

1. Introduction

Environmental concerns have led to new findings in chemical engineering that aim to reduce the carbon footprint and reach more sustainable processes. Extensive plant designs that generate large amounts of waste with sequential downstream units for the required treatment and high energy demand are real drawbacks in chemical manufacturing, to which the scientific community has given special attention. Photocatalysis has been considered a sustainable pathway to replace traditional routes, requiring less energy and allowing milder operating conditions. The synthesis of valuable compounds, such as aldehydes used in food, pharmaceutical and cosmetic sectors [1,2], has also shown promising results via photocatalytic processes. However, combining photo-assisted processes and effective catalysts with high productivity still requires a long pathway before industrial implementation. Therefore, organic synthesis via photocatalysis has gained exceptional thoughtfulness during the last decades [3], mainly using slurry photocatalytic systems. Due to the lower mass transfer limitations, suspended photocatalyst systems offer higher reaction rates than immobilised photocatalyst configurations [4]. However, the last one brings

* Corresponding author at: Laboratory of Separation and Reaction Engineering – Laboratory of Catalysis and Materials (LSRE-LCM), Faculty of Engineering, University of Porto, Rua Dr. Roberto Frias, Porto 4200-465, Portugal.
E-mail address: cgsilva@fe.up.pt (C.G. Silva).
[1] These two authors contributed equally to this work.
[2] Current affiliation: Colab Net4CO2- Network for a sustainable CO2 economy, UPTEC Asprela II- Rua Júlio de Matos, 828-882 4200-355 Porto, Portugal.

https://doi.org/10.1016/j.cattod.2024.115090
Received 5 August 2024; Received in revised form 2 October 2024; Accepted 5 October 2024
Available online 8 October 2024

significant benefits to the process design from the industrial and environmental point of view, reducing the downstream units and energy required for the photocatalyst recovery, meaning lower capital and operating costs. Considering the Process Intensification concept, the immobilisation of photocatalytic material is regarded as a fundamental key to safer and cleaner solutions. Besides, these systems can offer additional environmental advantages, owning to their possible reusability. On the other hand, using micro-mesostructured photoreactors provides a larger surface area per reaction volume. Additionally, these reactors achieve a higher spatial illumination homogeneity, allowing better light penetration than conventional large-scale reactors [5] and promoting photon transfer. Moreover, these structures present short molecular diffusion distances [6], minimising mass transfer resistances and benefitting the photocatalytic reaction.

The NETmix technology was first patented as a novel static mixer for the continuous production of hydroxyapatite nanoparticles [7,8]; lately, this structure has been explored for photocatalytic applications. The proof-of-concept was reported by Lima et al. [9] for removing antibiotics from aqueous solutions using the photo-Fenton process. Other studies were conducted, mainly related to air and water treatment [10–12]. Besides, it presents greater heat transfer capacity than the most common industrial microreactors [13]. Other significant advantages have been pointed out, such as the ability to efficiently control fluid mixture and flow distribution due to its regular network of chambers interconnected by transport channels. Thanks to its multi-injection scheme, versatility is an additional asset, which allows different feed configurations depending on the target product. Even under solar irradiation, outstanding performance with high reproducibility has also been reported [6,14]. Finally, this photoreactor offers easy scalability (in series or parallel) for large-scale continuous mode operation [15]. Its technological implementation is already well established, being an advantage from the industrial point of view for future commercial applications.

In this work, the NETmix structure was integrated with a light-emitting diode (LED) compact system and immobilised thin photocatalytic film to carry out selective oxidation reactions. As far as our knowledge goes, this approach was never explored for organic synthesis. A novel photocatalytic film was developed using different amounts of a metal-free photocatalyst, exfoliated graphitic carbon nitride, immobilised in a biodegradable matrix (sodium alginate). The photocatalytic performance of this new configuration was evaluated for the synthesis of some industrially essential aldehydes, namely anisaldehyde (AAD), tolualdehyde (TAD), benzaldehyde (BAD), vanillin (VAD) and piperonal (PAD) from the selective photocatalytic oxidation of their respective alcohols, anisyl (AA), toluyl (TA), benzyl (BA), vanillyl (VA) and piperonyl (PA) alcohols, respectively. Promising results were obtained even using environmentally friendly conditions, opening a new window for developing sustainable organic synthesis photocatalytic processes.

2. Experimental

2.1. Synthesis of photocatalytic films

The synthesis procedure of exfoliated carbon nitride (GCN-T) and its colloidal suspension (GCN-TS) has been previously reported [1] and is detailed in the Supplementary information (SI). The photocatalytic films were synthesised by adding 1 g of sodium alginate (SA) to 40 mL of UP-heated water at 50 ºC under constant stirring until the formation of a homogeneous paste. Afterwards, the desired amount of photocatalyst, GCN-T, was added to the paste with continuous stirring until the solid material was completely dispersed. Fig. SD1 illustrates the required steps for the synthesis of the photocatalytic film. After cooling it at room temperature, the thin photocatalytic film was prepared using the so-called doctor blade method. Finally, the moulds were immersed into a 3 wt% calcium chloride solution to obtain the hydrogel. The resulting films were denoted as xGCNT/SA, where x corresponds to the amount of GCN-T per 100 g of sodium alginate (e.g., 50GCNT/SA corresponds to a film with 0.5 g of GCN-T per 1 g of alginate). Moreover, different catalyst loads of GCN-TS were also added to the alginate hydrogel solution. The resulting material was labelled as xGCNTS/SA, where x corresponds to the amount of GCN-TS nanosheets (3.2, 6.4, 7.2, 9.6, 12.8 g) per 100 g of alginate (e.g., 3.2GCNTS/SA corresponds to a film with 32 mg of GCN-TS per 1 g of alginate).

2.2. Experimental setup

The reactions were conducted in the NETmix photoreactor equipped with an 18 LED lamp box (λ_{max} = 420 nm, 260 W m^2) at different flows (22–285 mL min^{-1}) in recirculation mode. The films were placed inside the reactor, covering all chambers except the inlets and the outlets. The alcohol solutions with a concentration of ca. 0.5 mM were used continuously, saturated with air. Fig. 1 presents a scheme of the reactional system layout, while the detailed schematic representation and description of the experimental setup used in all runs are depicted in Fig. SD 2.

3. Results and discussion

3.1. Catalyst characterisation

The characterisation of thermally exfoliated g-C_3N_4 (GCN-T) is well described in previous reports from our group [16,17]. The present work selected the most relevant characterisation to interpret the results, focusing on SA films with g-C_3N_4-based materials.

The chemical structure of the prepared films was inspected using spectroscopy to confirm the successful immobilisation of g-C_3N_4 on the SA matrix. The FTIR spectra of the SA film, GCN-T powder and GCNT/SA films are shown in Fig. 2a. The broad peak between 3575 and 3000 cm^{-1} in the SA sample films is attributed to -OH bonds. The peaks at 1590 and 1410 cm^{-1} correspond to asymmetrical and symmetrical vibrations related to the carboxylate ions. The band around 1000 cm^{-1} can be attributed to C-C and ether bonds [18]. The FTIR spectra of the GCN-T/SA prepared samples are very similar to those of SA films due to the low ratio of GCN-T material to the precursor sodium alginate. However, some characteristic peaks of GCN-T are observed, confirming the presence of g-C_3N_4 in the alginate film.

The bands at 1311 and 1235 cm^{-1} are attributed to the stretching vibration of C-N(-C)-C or C-NH-C linkage units [19]. The band at810 cm^{-1} corresponds to the vibration of the triazine ring [19].

Moreover, thermal analyses of dried films were conducted by thermogravimetry (TGA) (Fig. SD3). TGA results revealed that the GCNT/SA samples exhibited higher mass loss than SA, indicating that the incorporation of GCN-T affects the SA structure. Furthermore, the presence of GCN-T in the SA matrix enhances the thermal stability of the samples until approximately 630 °C. The main weight loss stage, occurring

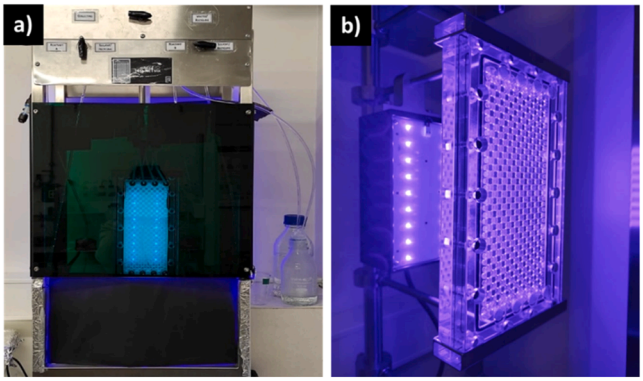

Fig. 1. (a) Front view of the LED-NETmix photoreactor pilot scale unit; (b) LEDs compact system (λ_{max} = 420 nm) irradiating the photoreactor.

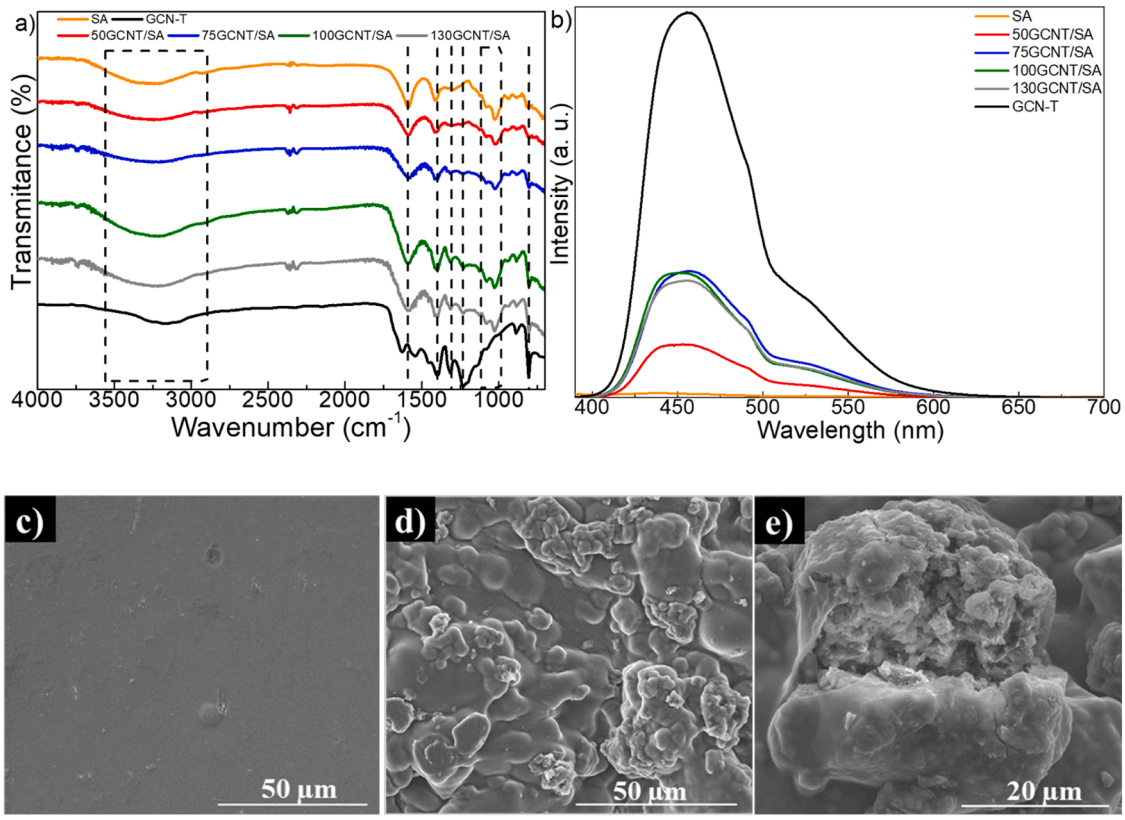

Fig. 2. (a) FTIR and (b) PL spectra of SA film, GCN-T powder and GCNT/SA films. SEM micrographs of the photocatalytic films: (c) SA, (d) 75GCNT/SA, (e) 75GCNT/SA (higher magnification).

between 540 °C and 660 °C, is attributed to the carbon nitride decomposition [20].

The optical properties of all GCNT/SA films were investigated by photoluminescence (PL) spectroscopy (Fig. 2b). Typically, in carbon nitride materials, the broad band observed at around ~ 433 nm is commonly attributed to electron-hole recombination, and the smaller emission band at around 528 nm is associated with surface defects of this type of photocatalyst [21–23]. The GCNT/SA samples exhibited distinctive patterns compared with the GCN-T powder material (Fig. 2b). Notably, the GCNT/SA samples reveal a reduced PL intensity compared to GCN-T powder material. A smaller PL intensity commonly indicates a reduced recombination rate of electron-hole pairs under light excitation [24,25]. However, the lower PL intensity observed in the GCNT/SA materials may be mainly ascribed to the interaction between the GCN-T powder and the SA matrix, which has a reduced PL intensity.

Diffuse reflectance UV-Vis (DRUV-Vis) analysis was conducted to further investigate the prepared films' optical properties (Fig. SD4a). The DRUV-Vis spectra of the GCNT/SA samples are very similar to the characteristic spectrum of g-C_3N_4 material between 300 and 450 nm. The DRUV-Vis spectra of the GCNT/SA materials were very similar, suggesting that the immobilisation process primarily attached the photocatalyst particles to the hydrogel matrix.

The morphology of thermally exfoliated g-C_3N_4 has been thoroughly described in our previous works [16,17,26]. The bulk g-C_3N_4 material typically exhibits a plate-like layered morphology composed of solid agglomerates, characteristic of a carbon nitride skeleton. Due to the thermal exfoliation, GCN-T material revealed thinner layers resulting from layer-by-layer thermal oxidation and layer splitting [17].

The SA and GCNT/SA films were morphologically characterised using scanning electron microscopy (SEM). Representative micrographs of both materials are presented in Fig. 2(c–e). SEM images show that the SA films exhibited a smooth and continuous surface (Fig. 2c). After incorporating GCN-T (Fig. 2d and e) into the alginate film, a uniform distribution of GCN-T particles across the SA film surface was observed. The GCN-T material tends to agglomerate, forming clusters or large particles wrapped by the polymer, as exhibited in the SEM images. The particles form agglomerations with higher dimensions when increasing the amount of GCN-T in the film (Fig. SD5).

Further ultrasonic exfoliation of GCN-T results in the formation of two-dimensional colloidal nanosheets constituted of a few atomic layers of g-C_3N_4 (GCN-TS) [27,28]. The resulting material, GCN-TS, whose characterisation can be found in previous works [6,40], was included in the SA matrix, resulting in GCNTS/SA films that were studied in this work.

The optical properties of the GCNTS/SA samples were evaluated by DRUV-Vis and PL spectroscopy. All prepared GCN-TS films exhibited similar DRUV-Vis and PL spectra profiles of the g-C_3N_4 (Fig. SD6a and b). Notably, in the DRUV-Vis spectra, the 12.8GCNTS/SA sample exhibited a second absorption band at 440 nm, which could be ascribed to the increase of the particle size due to the clustering of the nanosheets, resulting from concentrating the GCNTS colloidal suspension [29].

A blue-shift is noticed between 450 and 435 nm by comparing the PL spectra of SA films containing GCN-T and GCN-TS photocatalysts (Fig. SD7). This shift can be attributed to the decrease in carbon nitride layer thickness due to the exfoliation process [30], confirming the maintenance of the GCN-TS ultrathin structure after the immobilisation in the SA matrix.

The chemical structure of the prepared GCNTS/SA films was also inspected using FTIR spectroscopy (Fig. SD8). As also happened in the GCNT/SA samples, the FTIR spectra of GCNTS/SA films are very similar to that of SA due to the reduced quantity of photocatalyst used. Nevertheless, the characteristic peaks of g-C_3N_4 are detected even with a lower intensity, confirming the presence of GCN-TS supported on the SA polymer.

3.2. Photocatalytic synthesis of aromatic aldehydes using the NETmix photoreactor

Most processes for photocatalytic production of aromatic aldehydes utilising g-C_3N_4-based materials reported in the literature involve the material's dispersion in the reaction medium [16,31–33]. This method necessitates a post-separation step after the reaction to recover the photocatalyst and recover the products. In that case, some loss of photocatalyst may also occur between usages [34]. To address these challenges, immobilising the photocatalyst eliminates the need for separation processes and enables continuous production. Moreover, selecting an ideal photoreactor is crucial to enhance the photocatalytic efficiency of the system using an immobilised catalyst. The NETmix photoreactor design offers a significant advantage by providing a large area of irradiated photocatalyst per reaction volume, which is beneficial for using carbon nitride films.

The NETmix photoreactor was used for the oxidative conversion of AA to AAD with GCN-T catalysts immobilised in the SA polymer under visible-LED radiation. Before the light exposure, adsorption tests were performed using the GCNT/SA films. Control experiments using the SA film without the catalysts to evaluate the photochemical stability of the AA (Fig. SD 9). The results reveal that in the absence of the photocatalysts, the adsorption of the AA on the polymer surface can be considered negligent.

The effect of GCN-T content on the SA films was evaluated in terms of photocatalytic efficiency for the AA conversion to produce AAD using the NETmix photoreactor under ambient conditions. The photocatalytic activity of GCNT/SA films is illustrated in Fig. 3a, considering the AA conversion (X), the AAD selectivity (S) and yield (Y) when the maximum AAD yield was reached.

Comparing the results obtained for the photocatalytic synthesis of AAD using the prepared GCNT/SA samples, the maximum AAD yield obtained followed the order 75GCNT/SA > 100GCNT/SA > 130GCNT/SA > 50GCNT/SA. The maximum yield for AAD production (40 %) and AA conversion (77 %) was obtained after a 6 h reaction using 75GCNT/SA. The enhanced photocatalytic activity may be attributed to an optimal load of active photocatalyst available for light absorption and AA conversion. The lower performance of the 50GCNT/SA material may be ascribed9.6 to the lower amount of GCN-T present in the film. Above the GCNT/SA ratio of 0.75, the photocatalytic efficiency of the films starts to decrease. Higher GCN-T content promotes the formation of agglomerated GCN-T particles with higher dimensions in the polymer matrix, as observed in the SEM images (Fig. SD5). This can reduce the photocatalytic films' active area and light absorption capacity. So, it is possible to infer that there is a limit to the amount of GCN-T that could be immobilised onto the SA matrix without causing detrimental effects on AAD production [35]. Thus, the 75GCNT/SA film was selected for the following experiments.

Different flow rates were evaluated in the NETmix photoreactor, between 22 and 285 mL min^{-1}, corresponding to residence times of 0.96–0.11 min (Fig. SD10). The photocatalytic results were evaluated at the maximum AAD considering the values of the apparent rate constants (k_{app}) obtained for AA conversion, shown in Fig. SD10a. The kinetics of AA conversion using GCNT/SA films follow a pseudo-first-order model (Fig. SD10b). Up to a flow rate of 228 mL min^{-1}, the AAD yield and the k_{app} tend to increase. Increasing the flow rate and consequently decreasing the residence time, the AAD yield and k_{app} decrease to the same reaction time. Thus, it was possible to conclude that operating under a flow of 228 mL min^{-1} (residence time up to 0.14 min), a maximum AAD yield of 56 % was achieved after 1 h under visible light radiation.

The photocatalytic reaction performance mainly depends on the intrinsic properties of the catalyst, the chemical nature of the substrate, and the external mass transfer efficiency of the substrate from the liquid to the GCN-T/SA surface [36]. The external mass transfer efficiency can be determined by the flow rate that will define the contact between the reaction solution and the photocatalytic surface per unit of time [37]. Increasing the flow rate, the residence time decreases, which results in short contact between the solution and the immobilised catalysts, leading to a reduction in AA conversion.

The photocatalytic efficiency of the 75GCNT/SA film was evaluated for the conversion of different aromatic alcohols into the respective aldehydes using the NETmix reactor under a flow rate of 228 mL min^{-1}. The number, electronic maturity, and location of substituent groups attached to the aromatic ring significantly impact the reactivity of benzene derivatives [16,38]. Therefore, the relative ease of selectively synthesising the aromatic aldehydes under study may be rationalised by the relative ability of the parent chemical to be transformed according to the principles of photocatalytic oxidation of aromatic compounds. In this way, five different aromatic alcohols (AA, BA, PA, TA and VA) with various types and the location of substituent groups in the aromatic ring were used to produce the corresponding aromatic aldehydes (AAD, BAD, PAD, TAD and VAD). The presence of electron-donating (activating) or electron-withdrawing (deactivating) groups in the aromatic ring, respectively, may help or inhibit the photocatalytic conversion of such compounds [39]. Therefore, it stands to reason that the quantity, orientation, and type of substituent groups influence how much one aromatic alcohol converts compared to the others.

The concentration profiles of the aldehydes produced during the reactions are exhibited in Fig. 3b. In the dark period, a reduced concentration decrease of alcohol was observed, which confirms the negligible adsorption into the catalyst's surface (Fig. SD11a). All selected

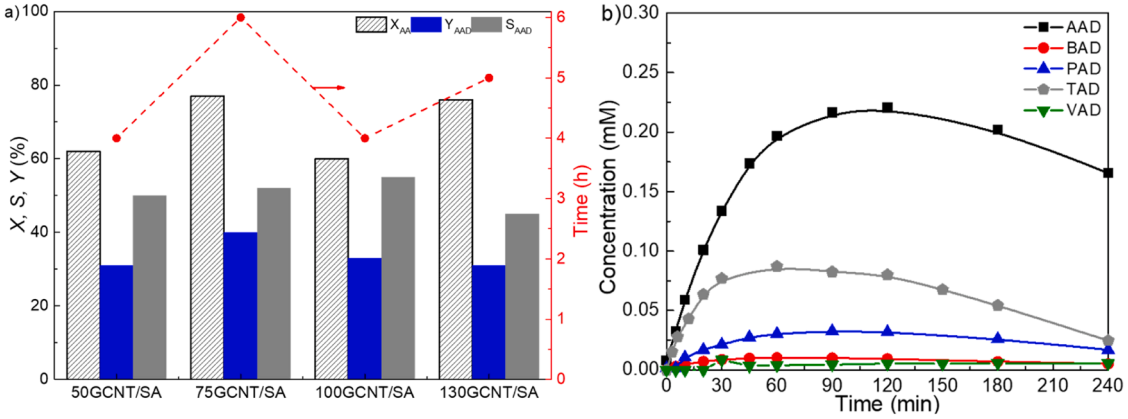

Fig. 3. (a) Conversion (X) of AA, selectivity (S), and yield (Y) for AAD formation using GCNT/SA and reaction time for the maximum yield of anisaldehyde (-●-). (b) Concentration profile of aromatic aldehydes AAD, BAD, PAD, TAD and VAD using 75GCNT/SA as catalyst. Reaction conditions: AA (0.5 mM), 228 mL min^{-1} flow, visible LED (λ_{max} = 420 nm).

aromatic alcohols were also expected to react insignificantly since they absorb only below 300 nm, thus being out of the emission band range of the irradiation source applied (Fig. SD 11b).

The maximum aldehyde production follows the order of AAD > TAD > PAD > BAD > VAD. After 120 min of irradiation, the maximum concentration of AAD (0.22 mM) was obtained, followed by the maximum produced of TAD (0.08 mM). As displayed in Fig. 3b, after reaching a maximum, the aldehyde concentration starts to decrease, which may result from over-oxidation. The main products that result from this degradative oxidation can be, for example, the anisic and vanillic acid in the case of anisaldehyde [39] and vanillin [16], respectively.

Among the five alcohols studied, AA showed faster conversion and AAD yield. The presence of a methoxy group (-OCH_3), an electron-donating group, on the para position will increase the electron density on the benzene ring and consequently increase the aromatic ring's stability, making it easier for the oxidation process. TA has two activating groups, methoxy- and methyl- (-CH_3), contributing to easy TAD production. BA only possesses a hydroxymethyl group, not benefiting from the electron-donor behaviour of the methoxy group, hence having a lower conversion and selectivity than AA and PA, which possesses a dioxole group, with electron-withdrawing properties, making the selective oxidation to PAD less likely to occur. Also, the overoxidation of piperonylic acid contributes to the low yield and selectivity [40]. VA possesses both strong electron-withdrawing groups, a methoxy group (-OCH_3) and a formyl group (-CHO), which decrease the electron density on the benzene ring, making the oxidation process less favourable and promote its destabilisation, resulting in the lowest VAD production yield.

As an attempt to improve the photocatalytic performance of the NETmix photoreactor for the production of AAD, films containing different catalyst loads of few-layer GCN (GCNTS/SA) were tested under the same reaction conditions. The photocatalytic performance quantified by considering the AA conversion, AAD selectivity, and yield after 180 min of radiation is illustrated in Fig. 4a. For comparison purposes, the results obtained with 75GCNT/SA are also shown.

The photocatalytic ability of GCNTS/SA samples for AA conversion as the catalyst load on the sodium alginate film increased. This tendency is also observed in terms of AAD selectivity and yield. The 12.8 GCNTS/SA sample is an exception to this tendency, which may be ascribed to a surplus amount of GCN-TS in the SA film, leading to particle agglomeration, as happened with the GCNT/SA samples. The best photocatalytic performance for the oxidative conversion of AA to AAD was obtained with the 9.6GCNTS/SA film, reaching 63 % of AA conversion, 39 % of AAD yield and 64 % of AAD selectivity after 180 min of visible light radiation. For comparison purposes, the 75GCNT/SA film was also tested in the same reaction conditions, and the results are also shown in Fig. 4a. After 180 min of irradiation, 81 % of AA conversion, 50 % and 39 % of AAD selectivity and yield were obtained, respectively.

To compare the effectiveness of the films prepared with GCN-T and GCN-TS, we calculated the ratio between the AAD produced and the catalyst mass in the SA polymer using the best-performing systems. This parameter establishes a relationship between the amount of catalyst used to produce the photocatalytic film of GCN-T and GCN-TS and its photocatalytic efficiency towards AAD production. The values of this parameter are 0.04 and 0.17 $mol_{AAD}\ g_{cat}^{-1}$ for 75CNT/SA and 9.6GCNTS/SA, respectively. Based on that, it is possible to conclude the 9.6GCNTS/SA film achieves better selectivity and yield with a lower mass of catalyst than the GCN-T film.

To evaluate the stability of the best performing system, the 9.6GCN-TS/SA sample was used in three reaction cycles, maintaining the reaction conditions. The catalytic film was exhaustively washed with UP water for 30 min between experiments.

As shown in Fig. 4b, from the first cycle of use to the second cycle, the photocatalytic film exhibits a decrease in the kinetic rate for the AA conversion and a reduction in the AAD production. The loss of the photocatalytic activity of the film can be related to the loss of some material after the washes. However, from the second to the third cycle, the efficiencies of the 9.6GCNTS/SA film remain practically constant, suggesting good photocatalytic and mechanical stability.

The 9.6GCNTS/SA morphology was evaluated after the reuses, and by the SEM images, it was possible to observe that a relatively high amount of GCN-TS nanoparticles was maintained dispersed on the sodium alginate surface (Fig. SD12a). No significant changes are observed in the film surface since the particle cluster wrapped by the polymer is maintained. A slight difference in PL spectra was found between the as-prepared and the used photocatalytic film (Fig. SD12b). This can be related to the minor part of GCN-TS that was partially lost, probably due to the several uses, manipulation and washing steps.

The results show that GCNTS/SA films present high stability and photocatalytic efficiency for AAD production. For the first time in this work, the NETmix technology was used for the photocatalytic synthesis of aromatic aldehydes. However, its application is still challenging from a technological point of view. The huge advantage of using a NETmix reactor is its ability to provide uniform light distribution and enhanced mass transfer, which are critical for optimising photocatalytic reactions. However, areas still require improvement, particularly regarding reactor design and process control. By incorporating advanced materials and improving the reactor configuration, it is possible to enhance the efficiency and selectivity of the photocatalytic process. In summary, while using NETmix technology for photocatalytic synthesis of aromatic aldehydes shows to be an excellent promise, relevant efforts in

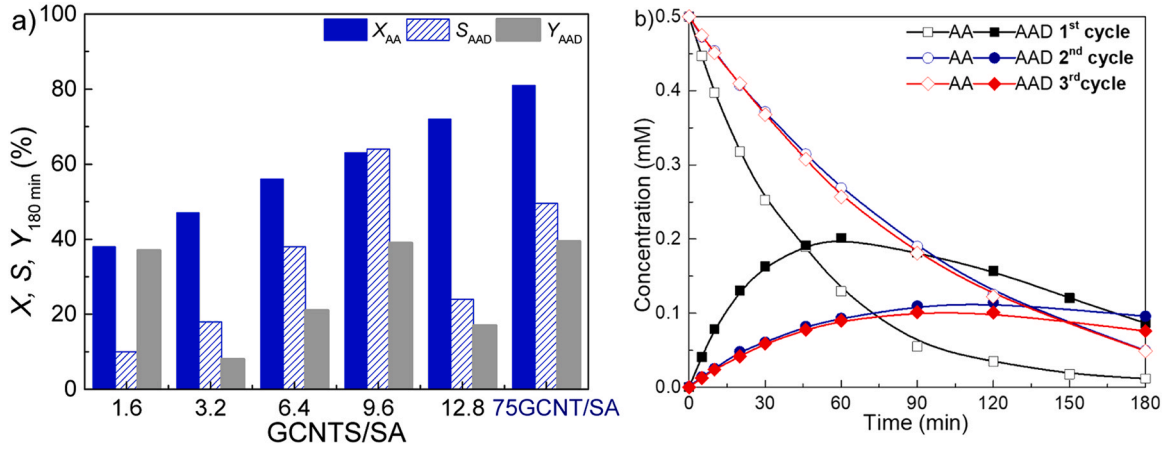

Fig. 4. (a) Conversion (*X*) for AA, selectivity (*S*) and yield (*Y*) for AAD formation using GCNTS/SA samples after 180 min of reaction; (b) Photocatalytic reutilisation reactions using 9.6GCNTS/SA film. Reaction conditions: AA (0.5 mM), 228 mL min^{-1} flow, visible LED (λ_{max} = 420 nm).

optimisation and innovation are still required to make it a viable and cost-effective solution for large-scale production.

4. Conclusions

For the first time, a novel NETmix photoreactor was used for the photocatalytic production of aromatic aldehydes. Biodegradable sodium alginate polymer was used as a matrix to support metal-free carbon nitride materials, eliminating the need for catalyst separation from the reaction medium after the photocatalytic processes, resulting in significant time and energy savings.

The best compromise between the amount of sodium alginate and exfoliated carbon nitride (GCN-T) was found in the 75GCNT/SA sample, which exhibited the best photocatalytic performance for the AA conversion and AAD production in aqueous medium within the NETmix photoreactor. A maximum AA yield of 40 % was reached using the 75GCNT/SA film under a flow of 228 mL min^{-1} after 6 h of visible irradiation.

By incorporating GCN-TS nanosheets into the SA matrix, it was possible to significantly reduce the catalyst amount (0.96 mg) required to prepare the films while increasing the photocatalytic efficiency. In this case, 63 % of AA conversion, 39 % of AAD yield and 64 % of AAD selectivity were obtained after 180 min of visible light radiation using the 9.6GCNTS/SA film. The stability of this material was confirmed for three successive runs.

Overall, this study demonstrated that immobilised carbon nitride photocatalysts in the sodium alginate matrix can effectively produce organic compounds through oxidative processes in aqueous phase. The operation using the NETmix photoreactor proved the versatility of the reaction system for various photocatalytic processes. Additionally, the adaptability of the hydrogel matrix for different reactions presents exciting possibilities for further research.

CRediT authorship contribution statement

Claudia Gomes Silva: Writing – review & editing, Supervision, Resources, Project administration, Methodology, Funding acquisition, Conceptualization. **Madalena M. Dias:** Resources, Methodology, Funding acquisition, Conceptualization. **Joaquim L. Faria:** Writing – review & editing, Supervision, Resources, Funding acquisition. **Dânia Constantino:** Writing – original draft, Methodology, Investigation, Conceptualization. **Joana C. Lopes:** Writing – review & editing, Writing – original draft, Methodology, Investigation, Conceptualization. **Rafael Carneiro:** Writing – original draft, Investigation. **José C.B. Lopes:** Writing – review & editing, Resources, Conceptualization.

Declaration of Competing Interest

The authors declare that they have no known competing financial interests or personal relationships that could have appeared to influence the work reported in this paper.

Data availability

Data will be made available on request.

Acknowledgements

This work was financially supported by national funds through FCT/MCTES (PIDDAC): LSRE-LCM, UIDB/50020/2020 (https://doi.org/10.54499/UIDB/50020/2020) and UIDP/50020/2020 (https://doi.org/10.54499/UIDP/50020/2020); ALiCE, LA/P/0045/2020 (https://doi.org/10.54499/LA/P/0045/2020); and by project SuN2Fuel (2022.04682.PTDC) with https://doi.org/10.54499/2022.04682.PTDC, funded by national funds through FCT/MCTES (PIDDAC). JCL acknowledges the PhD research grant from FCT, Ref. 2020.04651.BD (https://doi.org/10.54499/2020.04651.BD).

Appendix A. Supporting information

Supplementary data associated with this article can be found in the online version at doi:10.1016/j.cattod.2024.115090.

References

[1] J.C. Lopes, M.J. Sampaio, R.A. Fernandes, M.J. Lima, J.L. Faria, C.G. Silva, Outstanding response of carbon nitride photocatalysts for selective synthesis of aldehydes under UV-LED irradiation, Catal. Today (2019).
[2] G.K.T. Luong, Y. Ku, Selective oxidation of benzyl alcohol in the aqueous phase by TiO_2-based photocatalysts: a review, Chem. Eng. Technol. 44 (2021) 2178–2190.
[3] B. König, Photocatalysis in organic synthesis – past, present, and future, Eur. J. Org. Chem. 2017 (2017) 1979–1981.
[4] M. Dijkstra, A. Michorius, H. Buwalda, H. Panneman, J. Winkelman, A. Beenackers, Comparison of the efficiency of immobilized and suspended systems in photocatalytic degradation, Catal. Today 66 (2001) 487–494.
[5] H. Eskandarloo, A. Badiei, Fabrication of an inexpensive and high efficiency microphotoreactor using CO_2 laser technique for photocatalytic water treatment applications, Environ. Technol. 36 (2015) 1063–1073.
[6] B.A. Marinho, R. Djellabi, R.O. Cristóvão, J.M. Loureiro, R.A.R. Boaventura, M. M. Dias, J.C.B. Lopes, V.J.P. Vilar, Intensification of heterogeneous TiO_2 photocatalysis using an innovative micro–meso-structured-reactor for Cr(VI) reduction under simulated solar light, Chem. Eng. J. 318 (2017) 76–88.
[7] J.C.B. Lopes, P.E.S. Laranjeira, M.M.Q. Dias, A.A. Martins, Faculdade de Engenharia da Universidade do Porto, Netw. Mixer Relat. Mixing Process (2005).
[8] P.J. Gomes, V.M. Silva, P.A. Quadros, M.M. Dias, J.C. Lopes, A highly reproducible continuous process for hydroxyapatite nanoparticles synthesis, J. NanoSci. Nanotechnol. 9 (2009) 3387–3395.
[9] M.J. Lima, A.M.T. Silva, C.G. Silva, J.L. Faria, J.C.B. Lopes, M.M. Dias, An innovative static mixer photoreactor: proof of concept, Chem. Eng. J. 287 (2016) 419–424.
[10] B.A. Marinho, M.M. de Vidales, L.P. Mazur, L. Paulista, R.O. Cristóvão, D.A. Mayer, J.M. Loureiro, R.A. Boaventura, M.M. Dias, J.C.B. Lopes, Application of a micro-meso-structured reactor (NETmix) to promote photochemical UVC/H_2O_2 processes–oxidation of As (iii) to As (v), Photochem. Photobiol. 17 (2018) 1179–1188.
[11] S.G.S. Santos, L.O. Paulista, T.F.C.V. Silva, M.M. Dias, J.C.B. Lopes, R.A. R. Boaventura, V.J.P. Vilar, Intensifying heterogeneous TiO_2 photocatalysis for bromate reduction using the NETmix photoreactor, Sci. Total Environ. 664 (2019) 805–816.
[12] M.J. Lima, C.G. Silva, A.M.T. Silva, J.C.B. Lopes, M.M. Dias, J.L. Faria, Homogeneous and heterogeneous photo-Fenton degradation of antibiotics using an innovative static mixer photoreactor, Chem. Eng. J. 310 (2017) 342–351.
[13] M.F. Costa, C.M. Fonte, M.M. Dias, J.C.B. Lopes, Heat transfer performance of NETmix—a novel micro-meso structured mixer and reactor, AIChE J. 63 (2017) 2496–2508.
[14] B.M. da Costa Filho, A.L.P. Araujo, S.P. Padrão, R.A.R. Boaventura, M.M. Dias, J.C. B. Lopes, V.J.P. Vilar, Effect of catalyst coated surface, illumination mechanism and light source in heterogeneous TiO_2 photocatalysis using a mili-photoreactor for n-decane oxidation at gas phase, Chem. Eng. J. 366 (2019) 560–568.
[15] V.M. Silva, P.A. Quadros, P.E. Laranjeira, M.M. Dias, J.C. Lopes, A novel continuous industrial process for producing hydroxyapatite nanoparticles, J. Dispers. Sci. Technol. 29 (2008) 542–547.
[16] J.C. Lopes, M.J. Sampaio, R.A. Fernandes, M.J. Lima, J.L. Faria, C.G. Silva, Outstanding response of carbon nitride photocatalysts for selective synthesis of aldehydes under UV-LED irradiation, Catal. Today 357 (2020) 32–38.
[17] M.J. Lima, A.M.T. Silva, C.G. Silva, J.L. Faria, Graphitic carbon nitride modified by thermal, chemical and mechanical processes as metal-free photocatalyst for the selective synthesis of benzaldehyde from benzyl alcohol, J. Catal. 353 (2017) 44–53.
[18] J. Nastaj, A. Przewłocka, M. Rajkowska-Myśliwiec, Biosorption of Ni(II), Pb(II) and Zn(II) on calcium alginate beads: equilibrium, kinetic and mechanism studies, Pol. J. Chem. Technol. 18 (2016).
[19] B.V. Lotsch, M. Döblinger, J. Sehnert, L. Seyfarth, J. Senker, O. Oeckler, W. Schnick, Unmasking melon by a complementary approach employing electron diffraction, solid-state NMR spectroscopy, and theoretical calculations—structural characterization of a carbon nitride polymer, Chem. – A Eur. J. 13 (2007) 4969–4980.
[20] Y. Lu, C. Ji, Y. Li, R. Qu, C. Sun, Y. Zhang, Facile one-pot synthesis of C and g-C_3N_4 composites with enhanced photocatalytic activity using hydroxymethylated melamine as carbon source and soft template, Mater. Lett. 211 (2018) 78–81.
[21] G. Dong, K. Zhao, L. Zhang, Carbon self-doping induced high electronic conductivity and photoreactivity of g-C_3N_4, Chem. Commun. 48 (2012) 6178–6180.
[22] R. Godin, Y. Wang, M.A. Zwijnenburg, J. Tang, J.R. Durrant, Time-resolved spectroscopic investigation of charge trapping in carbon nitrides photocatalysts for hydrogen generation, J. Am. Chem. Soc. 139 (2017) 5216–5224.
[23] Y. Wang, M.K. Bayazit, S.J.A. Moniz, Q. Ruan, C.C. Lau, N. Martsinovich, J. Tang, Linker-controlled polymeric photocatalyst for highly efficient hydrogen evolution from water, Energy Environ. Sci. 10 (2017) 1643–1651.

[24] W.I. Nawawi, R. Zaharudin, M.A.M. Ishak, K. Ismail, A. Zuliahani, The preparation and characterization of immobilized TiO_2/PEG by using DSAT as a support binder, Appl. Sci. 7 (2017).
[25] F.B. Li, X.Z. Li, Photocatalytic properties of gold/gold ion-modified titanium dioxide for wastewater treatment, Appl. Catal. A: Gen. 228 (2002) 15–27.
[26] M.J. Lima, P.B. Tavares, A.M.T. Silva, C.G. Silva, J.L. Faria, Selective photocatalytic oxidation of benzyl alcohol to benzaldehyde by using metal-loaded g-C_3N_4 photocatalysts, Catal. Today 287 (2017) 70–77.
[27] S. Yang, Y. Gong, J. Zhang, L. Zhan, L. Ma, Z. Fang, R. Vajtai, X. Wang, P. M. Ajayan, Exfoliated graphitic carbon nitride nanosheets as efficient catalysts for hydrogen evolution under visible light, Adv. Mater. 25 (2013) 2452–2456.
[28] M.J. Lima, A.M.T. Silva, C.G. Silva, J.L. Faria, A microfluidic reactor application for the continuous-flow photocatalytic selective synthesis of aromatic aldehydes, Appl. Catal. A: Gen. 608 (2020) 117844.
[29] Y. Chen, B. Wang, S. Lin, Y. Zhang, X. Wang, Activation of n → π* transitions in two-dimensional conjugated polymers for visible light photocatalysis, J. Phys. Chem. C 118 (2014) 29981–29989.
[30] R.A. Fernandes, M.J. Sampaio, G. Dražić, J.L. Faria, C.G. Silva, Efficient removal of parabens from real water matrices by a metal-free carbon nitride photocatalyst, Sci. Total Environ. 716 (2020) 135346.
[31] M. Ilkaeva, I. Krivtsov, J.R. García, E. Díaz, S. Ordóñez, E.I. García-López, G. Marcì, L. Palmisano, M.I. Maldonado, S. Malato, Selective photocatalytic oxidation of 5-hydroxymethyl-2-furfural in aqueous suspension of polymeric carbon nitride and its adduct with H_2O_2 in a solar pilot plant, Catal. Today 315 (2018) 138–148.
[32] M. Ilkaeva, I. Krivtsov, E.I. García-López, G. Marcì, O. Khainakova, J.R. García, L. Palmisano, E. Díaz, S. Ordóñez, Selective photocatalytic oxidation of 5-hydroxymethylfurfural to 2,5-furandicarboxaldehyde by polymeric carbon nitride-hydrogen peroxide adduct, J. Catal. 359 (2018) 212–222.
[33] I. Krivtsov, E.I. García-López, G. Marcì, L. Palmisano, Z. Amghouz, J.R. García, S. Ordóñez, E. Díaz, Selective photocatalytic oxidation of 5-hydroxymethyl-2-furfural to 2,5-furandicarboxyaldehyde in aqueous suspension of g-C_3N_4, Appl. Catal. B: Environ. 204 (2017) 430–439.
[34] P.E. Laranjeira, A.A. Martins, J.C.B. Lopes, M.M. Dias, NETmix®, a new type of static mixer: modeling, simulation, macromixing, and micromixing characterization, AIChE J. 55 (2009) 2226–2243.
[35] Z.A.M. Hir, P. Moradihamedani, A.H. Abdullah, M.A. Mohamed, Immobilization of TiO_2 into polyethersulfone matrix as hybrid film photocatalyst for effective degradation of methyl orange dye, Mater. Sci. Semicond. Process. 57 (2017) 157–165.
[36] H. Kim, H. Kwon, R. Song, S. Shin, S.-Y. Ham, H.-D. Park, J. Lee, P. Fischer, E. Bodenschatz, Hierarchical optofluidic microreactor for water purification using an array of TiO_2 nanostructures, npj Clean. Water 5 (2022) 62.
[37] T. Razzaq, C.O. Kappe, Continuous flow organic synthesis under high-temperature/pressure conditions, Chem. – Asian J. 5 (2010) 1274–1289.
[38] M.J. Sampaio, C.G. Silva, A.M. Silva, V.J. Vilar, R.A. Boaventura, J.L. Faria, Photocatalytic activity of TiO_2-coated glass raschig rings on the degradation of phenolic derivatives under simulated solar light irradiation, Chem. Eng. J. 224 (2013) 32–38.
[39] G. Palmisano, M. Addamo, V. Augugliaro, T. Caronna, A. Di Paola, E.G. López, V. Loddo, G. Marcì, L. Palmisano, M. Schiavello, Selectivity of hydroxyl radical in the partial oxidation of aromatic compounds in heterogeneous photocatalysis, Catal. Today 122 (2007) 118–127.
[40] M. Bellardita, V. Loddo, G. Palmisano, I. Pibiri, L. Palmisano, V. Augugliaro, Photocatalytic green synthesis of piperonal in aqueous TiO_2 suspension, Appl. Catal. B: Environ. 144 (2014) 607–613.